Supplementary material

Two-dimensional layered Janus-In_2SeTe/C_2N van der Waals heterostructures for photocatalysis and photovoltaics: First-principles calculations

Xiao-Hua Li,[a] Bao-Ji Wang,*[a] Hui Li,[a] Xue-Feng Yang,[a] Rui-Qi Zhao,[b] Xing-Tao Jia,[a] and San-Huang Ke*[c]

[a]School of Physics and Electronic Information Engineering, Henan Polytechnic University, Jiaozuo 454000, China

[b]School of Materials Science and Engineering, Henan Polytechnic University, Jiaozuo 454000, China

[c]MOE Key Labortoray of Microstructured Materials, School of Physics Science and Engineering, Tongji University, Shanghai 200092, China

*Corresponding author: wbj@hpu.edu.cn

*Corresponding author: shke@tongji.edu.cn

1. The band structure and electrostatic potentials with/without dipole corrections

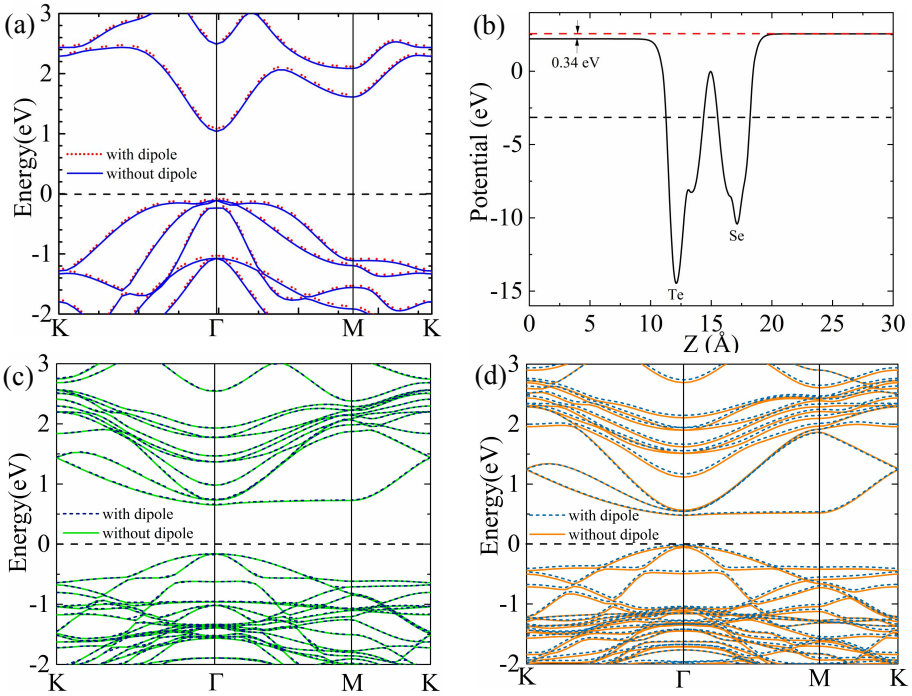

Fig. S1. (a) The band structure and electrostatic potentials of Janus In2SeTe monolayer with/without dipole corrections applied. (b) The electrostatic potentials of Janus In_2SeTe monolayer with dipole corrections applied. Band structures (c) $TeIn_2Se/C_2N$, (d) $SeIn_2Te/C_2N$ heterostructure obtained with/without dipole corrections. All results are calculated with PBE functional.

2. Two types of the heterostructures fabricated by Janus-In_2SeTe and C_2N monolayers

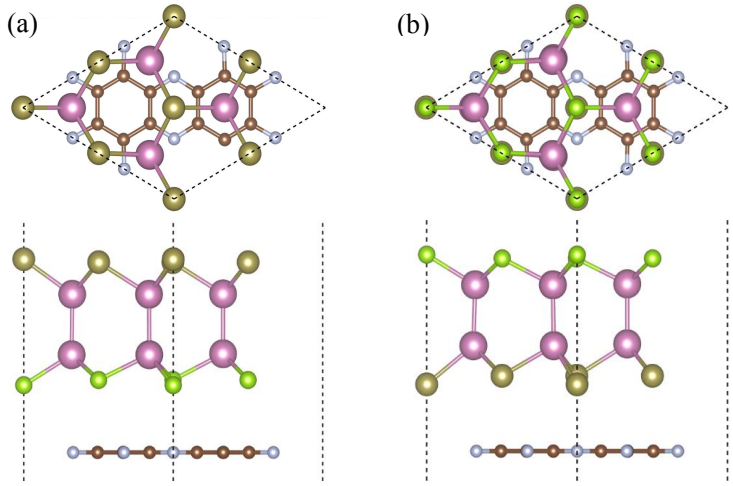

Fig. S2. Top and side views of (a) $TeIn_2Se/C_2N$ and (b) $SeIn_2Te/C_2N$ vdWHs with γ-stacking configuration.

3. The molecular dynamics simulations of Janus-In_2SeTe/C_2N vdWHs

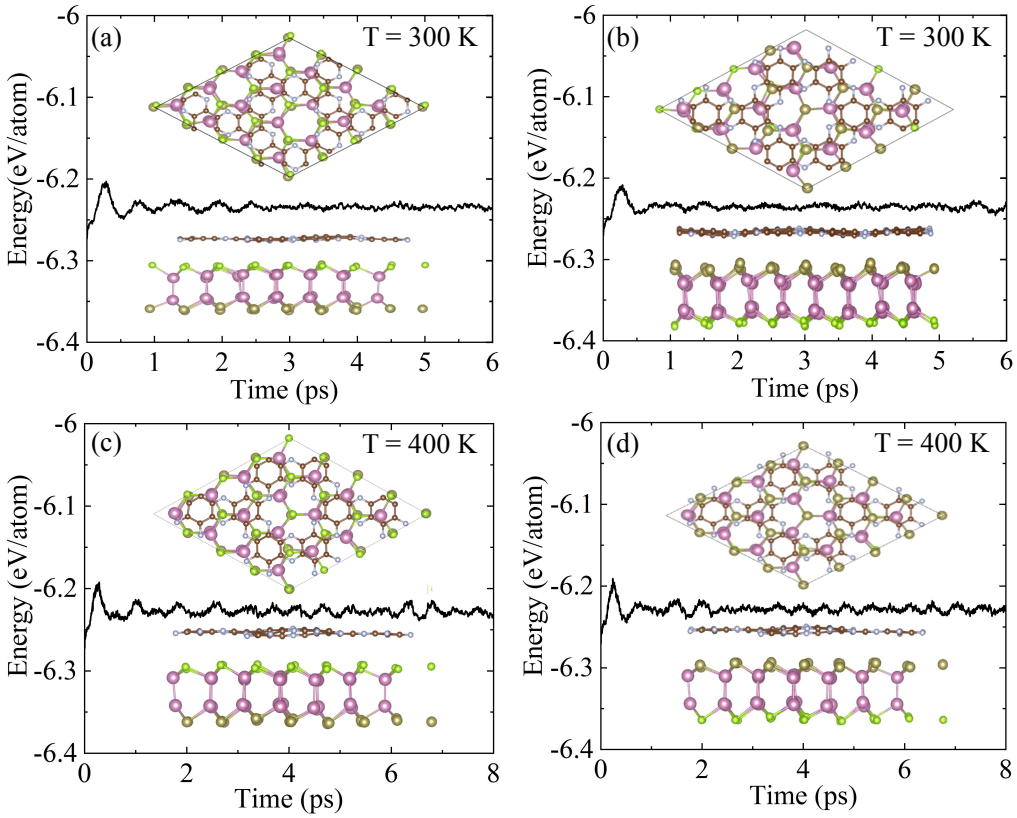

Fig. S3. The results of molecular dynamics simulation of (a,c) $TeIn_2Se/C_2N$ and (b,d) $SeIn_2Te/C_2N$ heterostructures.

4. The exciton binding energies of Janus-In_2SeTe/C_2N vdWHs and their components

Table S1: Macroscopic static dielectric constants and exciton binding energies of Janus-In_2SeTe, C_2N monolayers and Janus-In_2SeTe/C_2N heterostructures

	ε_{ion}			ε_{el}			E_{eb}
	x	*y*	*z*	*x*	*y*	*z*	
C_2N	2.73	2.73	1.13	0.04	0.04	0.01	1.14
In_2SeTe	3.24	3.24	1.34	0.96	0.96	0.01	0.10
$TeIn_2Se/C_2N$	4.03	4.03	1.45	1.02	1.02	0.02	0.12
$SeIn_2Te/C_2N$	4.06	4.05	1.45	1.08	1.08	0.02	0.14

5. The band structures and alignments of InSe/C_2N and InTe/C_2N vdWHs

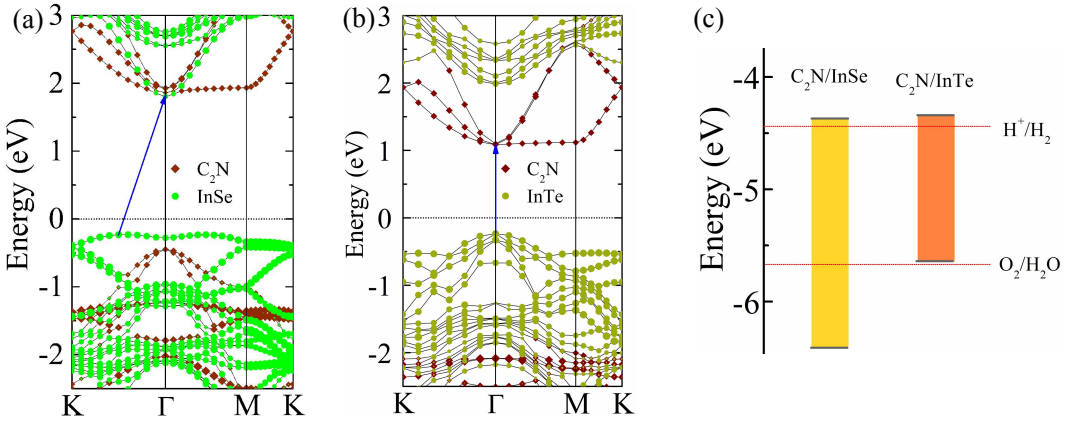

Fig. S4. The band structures of (a) InSe/C_2N and (b) InTe/C_2N heterostructures and (c) their band alignments. The redox potentials of water splitting at pH 0 (red dotted line) is shown for comparison.

6. Computational detail of the carrier mobility

Using the acoustic phonon limited method, we quantitatively estimate the carrier mobility for Janus-In_2SeTe/C_2N vdWHs and their parent monolayers. In 2D materials, the carrier mobility can be calculated by the formula [1-2]

$$\mu_{2D} = \frac{2e\hbar^3 C_{2D}}{3k_B T\left|m^*\right|^2 (E_l^i)^2}$$

where e, $\hbar$, k_B and T is the electron charge, reduced Planck constant, Boltzmann constant and temperature, respectively. The temperature is set to be 300 K in the calculations. C_{2D} is the in-plane stiffness of 2D material calculated by $C_{2D} = (\partial^2(E - E_0)/\partial\varepsilon^2)/S$, where $E - E_0$ is the total energy shift activated by strain effect and S is the equilibrium area, $m*$ is the effective mass in the transport direction for the electron or hole, which can be obtained by $m^* = \hbar^2(\partial^2 E/\partial k^2)^{-1}$. E_l^i is the deformation potential constant of the valence band maximum (VBM) for holes and conduction band minimum (CBM) for electrons along the transport direction, defined by $E_l^i = \Delta V_i/(\Delta l/l_0)$, in which ΔV_i is the energy change of the i band under proper cell compression and dilatation, l_0 is the lattice constant in the transport direction, and Δl is the deformation of l_0.

For convenience, orthorhombic lattices instead of pristine hexagonal lattices are used to calculate the uniaxial strain responses along x and y directions, as shown in Fig. S5. The $m*$ of electrons and holes are calculated by fitting parabolic functions to CBM and VBM along the transport direction. Then, the C_{2D} and E_l^i are obtained by parabolic fitting of the total energy shift and linearly fitting of the band edge positions of the VBM and CBM as a function of the uniaxial strain along x and y directions, respectively (see Fig. S6 and S7).

[1] Z. Guo, J. Zhou, L. Zhu, Z. Sun, Mxene: A promising photocatalyst for water splitting, J. Mater. Chem. A 4 (2016) 11446–11452.
[2] J. Dai, X. C. Zeng, Titanium trisulfide monolayer: Theoretical prediction of a new direct-gap semiconductor with high and anisotropic carrier mobility, Angew. Chem. Int. 54 (2015) 7572–7576.

7. Orthorhombic lattices of Janus-In_2SeTe/C_2N vdWHs and their parent monolayers

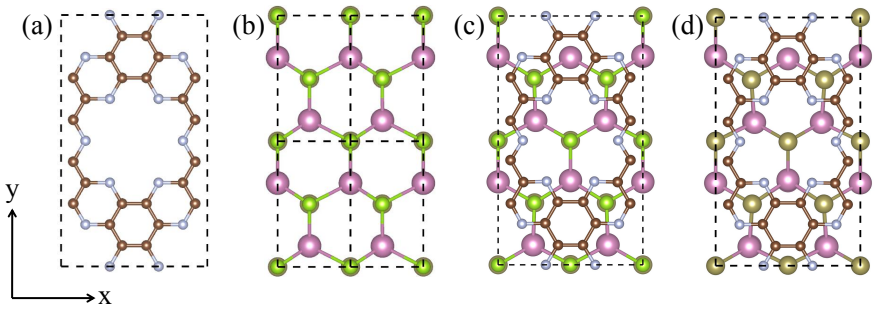

Fig. S5. The orthorhombic lattices used to calculate the uniaxial strain responses along *x* and *y* directions for (a) C_2N, (b) Janus-In_2SeTe monolayers, (c) $TeIn_2Se/C_2N$, (d) $SeIn_2Te/C_2N$ vdWHs.

8.The elastic modulus and the deformation potential calculations of C_2N and Janus-In_2SeTe monolayers

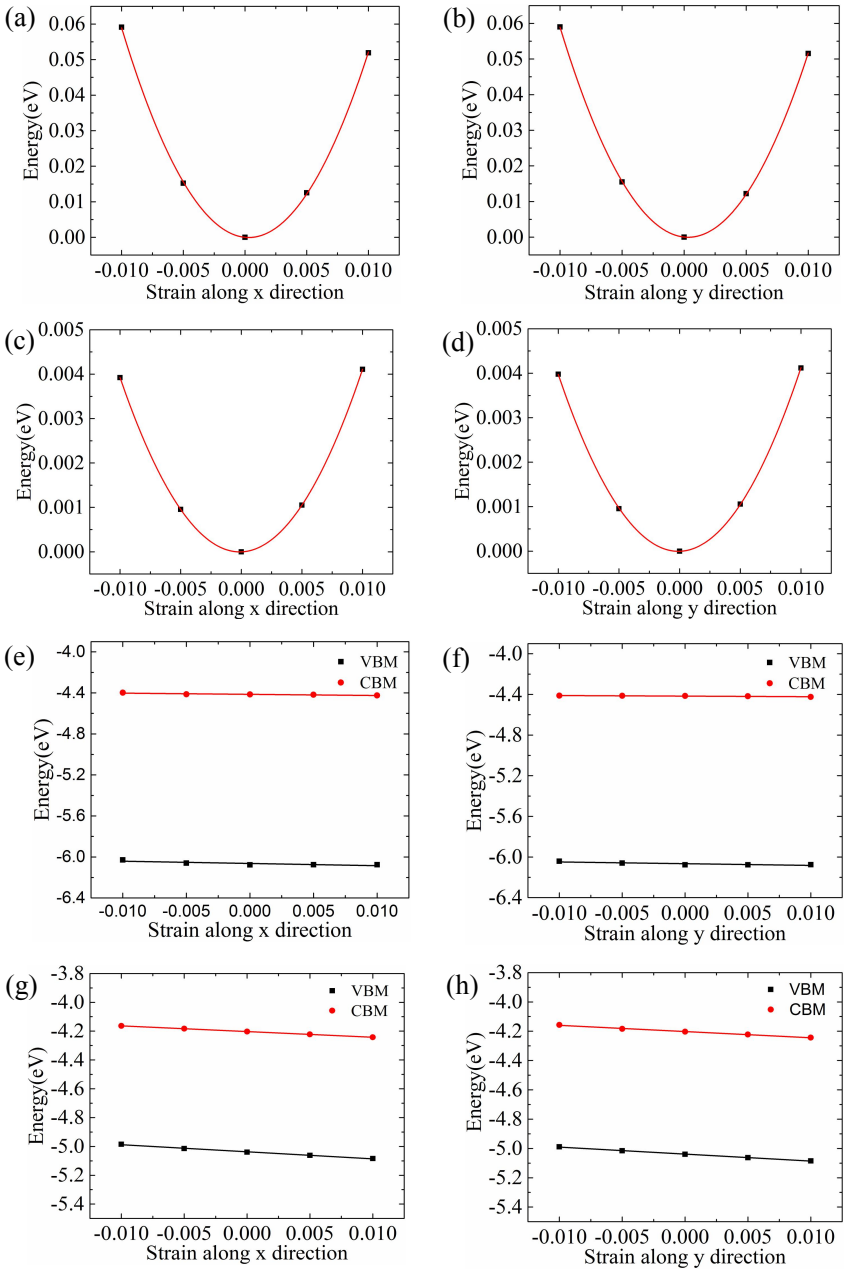

Fig. S6. The relationship between energy and strain for (a,b) C_2N and (c,d) In_2SeTe monolayers. The CBM and VBM along the x and y directions as a function of deformation proportion for (e,f) C_2N and (g,h) In_2SeTe monolayers.

9. The elastic modulus and the deformation potential calculations of Janus-In_2SeTe/C_2N vdWHs

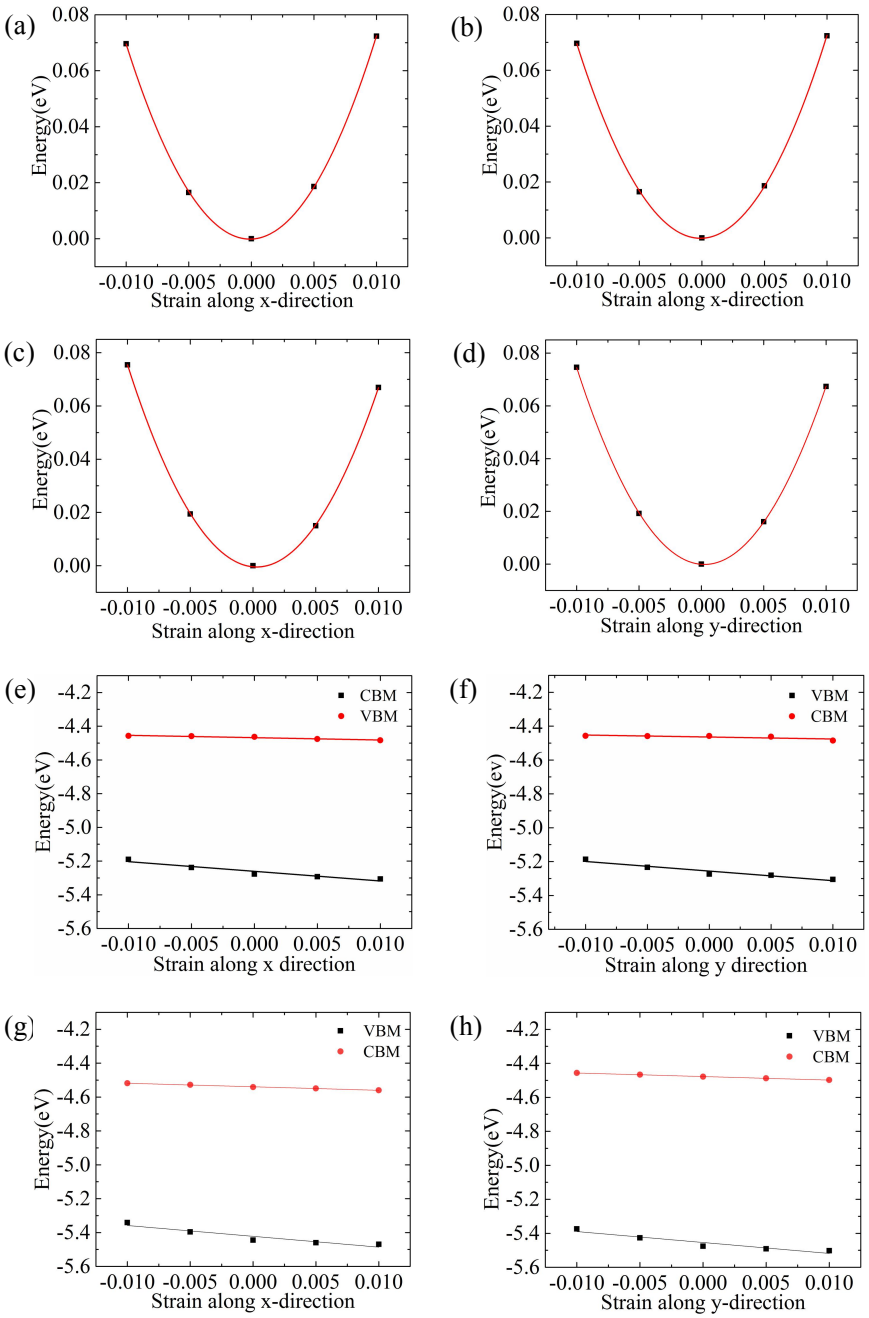

Fig. S7. The relationship between energy and strain for (a,b) $TeIn_2Se/C_2N$ and (c,d) $SeIn_2Te/C_2N$ vdWHs. The CBM and VBM along the x and y directions as a function of deformation proportion for (e,f) $TeIn_2Se/C_2N$ and (g,h) $SeIn_2Te/C_2N$ vdWHs.

10. Discussion S1:

As we know, in contrast to the quasiparticle selfconsistent GW method, the hybrid functional calculations (HSE) could underestimate the band gap of semiconductors. Meanwhile, we noted that the electronic structures of 2D Te-based semiconductors and Janus structures can be affected by the spin-orbital coupling (SOC) effect [Phys. Chem. Chem. Phys. 2018, 20, 18571-18578]. To check the quality of the HSE06 functional adopted in this work, we performed test calculations for Janus-In2SeTe monolayer using HSE06 and G0W0 functionals with/without SOC correction. The bandgap obtained with G_0W_0 is 2.28 eV, while G_0W_0+SOC gives a result of 1.97 eV, which is slightly higher than the HSE06 value (1.82 eV) obtained in our work. Indeed, higher level functionals may result in more accurate result. Unfortunately, the G_0W_0+SOC method is computationally very expensive and thus out of reach when large data sets of periodic systems are studied, as done in this work, especially for the heterostructure systems. Thus, the HSE06 method is probably a good option in our work. Of course, for future related experimental studies, the band gaps obtained in this work should be taken with care since it is likely is slightly underestimated.